

Estimation of the ages of Devonian and Cretaceous stage boundaries in the Geologic Time Scale

F. P. Agterberg⁽¹⁾, F. M. Gradstein⁽²⁾ and A.S. Gale⁽³⁾

(1) Geological Survey of Canada, Ottawa, Ontario, Canada.
frits@rogers.com

(2) Natural History Museum, University of Oslo, 0318 Oslo, Norway.
felix.gradstein@gmail.com

(3) School of Environment, Geography and Geological Sciences, University of Portsmouth, Burnaby Building, Burnaby Road, Portsmouth PO13QL, U.K.
andy.gale@port.ac.uk

ABSTRACT

Estimation of the ages of period and stage boundaries of the Geologic Time Scale (GTS) has a long history that commenced over a century ago with the pioneering work of Arthur Holmes. Frequencies, precision and accuracy of radiogenic isotope age determinations used for time scale construction continue to increase steadily. Later stage boundary age estimates are accompanied by error bars based on 2-sigma age dating errors with incorporation of stratigraphic uncertainty. Most GTS2004 and GTS2012 results involved spline-curve fitting. In GTS2012, Milankovitch-type orbital climate cyclicity was used to tune the Neogene geologic time scale while seafloor spreading was combined with sedimentary cycle scaling to construct the Paleogene time scale, and it also contributed to the construction of the Cretaceous and Jurassic time scales. Geomathematical procedures continue to be refined for the next GTS which is in Gradstein *et al.* (2020). In this study smoothing splines are used to construct Devonian and Late Jurassic- Early Cretaceous time scales. This methodology and its results are described and some estimates are refined by incorporating Milankovitch cycle durations.

Keywords: GTS2012, spline-curve fitting, Neogene, Milankovitch cycles.

Estimación de las edades de los límites de los pisos del Devónico y Cretácico en la Escala de Tiempo Geológico

RESUMEN

La estimación de las edades de los límites de períodos y pisos de la Escala de Tiempo Geológico (GTS) tiene una larga historia que comenzó hace aproximadamente un siglo con el trabajo pionero de Arthur Holmes. La frecuencia, precisión y fiabilidad de las dataciones por isótopos radiogénicos siguen mejorando continuamente. Las últimas estimaciones de la edad de los límites de pisos se vienen acompañando por barras de error basadas en 2-sigma de los errores de datación con la incorporación de la incertidumbre estratigráfica. La mayoría de los resultados de GTS2004 y GTS2012 requirió de ajuste de curvas por splines. En GTS2012, la ciclicidad climática por causas orbitales, del tipo ciclos de Milankovitch se utilizaron para tunear la Escala de Tiempo Geológico del Neógeno mientras que la expansión del fondo del océano se combinó con el escalado de ciclos sedimentarios para construir la escala temporal del Paleógeno, y contribuyó también a la construcción de las escalas temporales del Jurásico y Cretácico. Los procedimientos geomatemáticos continúan refinándose para la próxima GTS que está en prensa. En este estudio se usa el suavizado por splines para construir las escalas temporales del Devónico y Jurásico Superior-Cretácico Inferior y algunas estimaciones se refinan mediante la incorporación de la duración de los ciclos de Milankovitch.

Palabras clave: GTS2012, ajuste de curvas, splines, Neogeno, ciclos de Milankovitch.

Introduction

Various methods have been used in the past for estimating the numerical geologic time scale (GTS). Comprehensive reviews were given in the geomathematical method chapters of GTS2004 (Gradstein et al. eds., 2004) and GTS2012 (Gradstein et al. eds., 2012). For Paleozoic periods in these two earlier GTS publications, time scale construction included fitting a cubic smoothing spline curve (Agterberg, 2004; Agterberg et al., 2012). A new version of this technique (see later in this study) is also used for GTS2020 as shown in Figures 1 to 3 where the age determinations are plotted in the vertical direction (along the *y*-axis) against relative stratigraphic position (*x*-axis). The error bars shown are ± 2-sigma for the age determinations and widths of rectangular uncertainty boxes for the stratigraphic positions. The resulting uncertainty crosses in Figures 1 to 3 provide a simple check on how well the original data are in accordance with the best-fitting spline curve. On average one would expect that only about 5% of these crosses do not intersect the curve. This simple goodness-of-fit test is passed for both spline curves. Figures 1-3 as well as most other figures and tables in this paper are taken from Gradstein et al. (eds., in press).

To some extent, the scale initially used for relative stratigraphic position determines the shape of the final spline curve fitted to the age determinations. A relative stratigraphic scale should be used that is as close as possible to the numerical geologic time scale (in millions of years) except for a linear transformation. Less satisfactory relative stratigraphic scales used in the past included scales based on sediment accumulation corrected for differences in rates of sedimentation, the hypothesis of equal duration of stages (Harland et al., 1982), and the hypothesis of equal duration of biozones (Kent and Gradstein, 1986; Harland et al., 1990; Gradstein et al., 1995).

Unless the stratigraphic uncertainty can be neglected in the spline fitting, each age determination is weighted according to the inverse of its variance $s^2_i(y) = s^2_2(x) + s^2(y)$ corresponding to variances for stratigraphic uncertainty and based on the published 2-sigma error bars. The rationale behind this relatively simple transformation is that the *x*-axis also represents a time scale with rectangular error boxes of width *q* and $s(x) = 1.15 \cdot q/4$ (cf. Agterberg, 2002). Ideally, when stratigraphic standard deviations $s(x_i)$ are combined with $s(y_i)$ values, x_i and y_i as well as $s(x_i)$ and $s(y_i)$ are expressed in millions of years and the line of best fit would have the simple equation $y = x$.

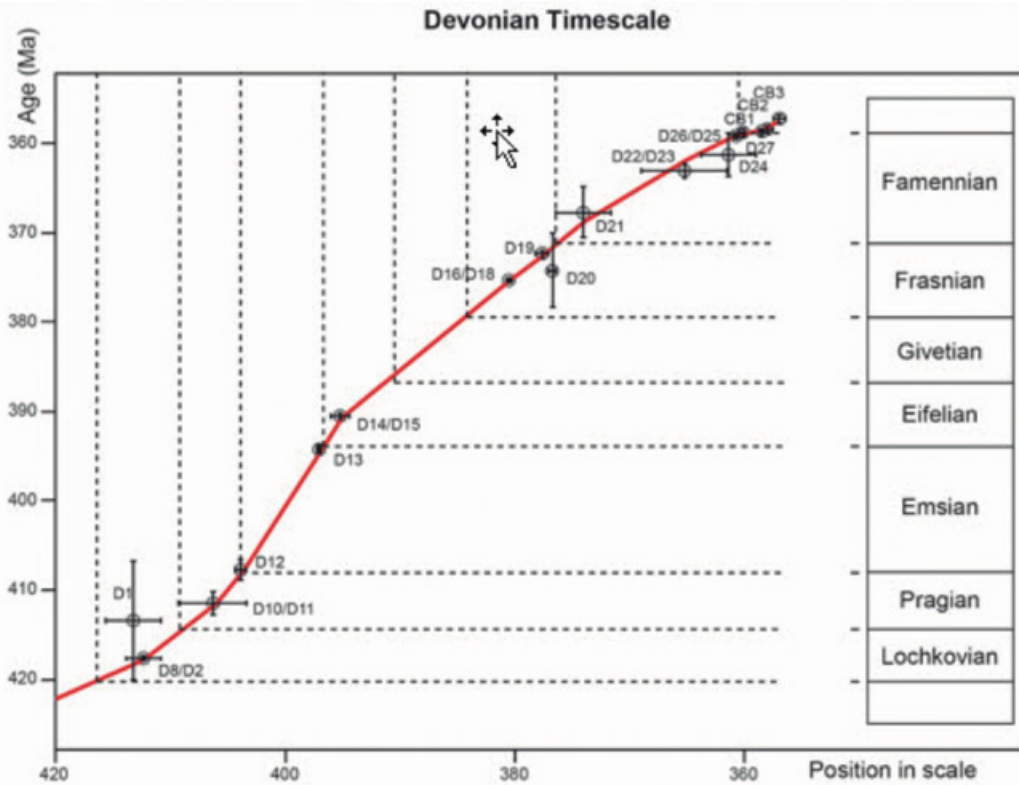


Figure 1. Best-fitting spline-curve for the Devonian in GTS2020.

Figura 1. Mejor ajuste de curvas por splines para el Devónico en GTS2020.

A cubic-smoothing spline $f(x)$ is fully determined by n pairs of values (x_i, y_i) , the standard deviations of the dates $s(y_i)$, and a smoothing factor (SF) representing the square root of the average value of the squares of scaled residuals $r_i = (y_i - f(x_i))/s(y_i)$. The method of "leaving-out-one" cross-validation (Agterberg, 2004) can be used to determine the optimum smoothing factor. In this method, all observed dates y_i , between the oldest and youngest one, are successively left out from spline fitting with pre-selected trial values of SF. The result is $(n - 2)$ spline curves for each SF tried.

In our GTS2020 applications use was made of the R-program *smooth.spline* as implemented by B.D. Ripley and M. Maechler in R.Stats Package version 3.6.0, with uncertainties based on total variance. This R program is freely available on the internet and widely used. Originally, the current spline-fitting technique was based on code in the GAMBIT FORTRAN program by Hastie and Tibshirani (1990) using a smooth-spline function similar to the one described in Chambers and Hastie (1992). The default application in R *smooth.spline* is application of a technique called generalized cross-validation (GCV). This technique was originally introduced by Wahba (1985) as a possible refinement of leaving-one-out cross-validation (CV). Differences between CV and GCV are discussed by Wang (2011). Usually the two methods give approximately the same results. However, in several of our applications to Paleozoic data sets, CV provided better results than GCV. This is because it is more robust in situations that relatively many points along the x -axis are relatively close together. In such situations, CV produces a smooth curve whereas the GCV result may reduce to a set of straight line segments connecting neighboring points. Best-fitting smooth curves were obtained by CV in all GTS2020 applications.

Schwarzacher (1993) was one of the pioneers in advocating use of the Milankovitch theory in cyclostratigraphy. In GTS2012, Milankovitch-type orbital climate cyclicity was already used to tune the Neogene

geologic time scale while seafloor spreading was combined with sedimentary cycle scaling to construct the Paleogene time scale. In GTS2020, orbital climate cyclicity applications for the Neogene and Paleogene and further improved and Milankovitch cycles are used for spline-fitting to obtain the Late Cretaceous time scale.

In this study smoothing splines will be used to construct revised Devonian and Late Jurassic - Early Cretaceous time scales. To some extent the spline estimates of the ages of stage boundaries for these two systems are refined by incorporating Milankovitch cycle durations. The main reason for taking the Devonian for example in this paper is that relatively few age determinations are available for it because of lack of ash layers in the Late Eifelian, the entire Givetian and the Early Frasnian. This called for consideration of the relative abundance of dates over time in the spline-fitting, in addition to consideration of the age determination errors and the stratigraphic uncertainty. A new method based on so-called hot spot analysis will be introduced for the Devonian to incorporate this third kind of uncertainty.

Devonian Splines

In comparison with other Paleozoic periods, relatively few age determinations continue to be available for the Devonian. For GTS2012, a bootstrap method was used obtaining an average spline curve based on 10,000 individual splines each based on random sampling of random variables for all dates with normal (Gaussian) distributions in the y -direction and rectangular distributions in the x -direction. The Devonian also has been the subject of a study by de Vleeschouwer and Parnell (2014) who applied a different method (Bchron) for deriving the curve relating the age determinations to the stratigraphic scale. In this section special attention is paid to the Devonian, which has a notable lack of

Base of Stage	GTS2012 Age (Ma)	GTS2020 Age (Ma)	Bchron-2014 Age (Ma)
Tournaisian	358.9 ± 0.4	359.3 ± 0.3	359.1 ± 0.4
Famennian	372.2 ± 1.6	371.4 ± 0.6	372.8 1.8/-3.2
Frasnian	382.7 ± 1.0	379.0 ± 0.9	382.5 3.5/-2.6
Givetian	387.7 ± 0.8	385.9 ± 1.5	387.4 1.8/-3.3
Eifelian	393.3 ± 1.2	394.2 ± 1.6	394.9 ± 2.6
Emsian	407.6 ± 2.6	407.9 ± 1.0	407.6 4.3/-2.5
Pragian	410.8 ± 2.8	414.4 ± 1.1	411.0 ± 3.5
Lochkovian	419.2 ± 3.2	420.0 ± 0.9	418.8 ± 2.7

Table 1. Summary of interpolated ages of Devonian epoch and stage boundaries. Radiometric age-dates (after Agterberg et al, 2020).

Tabla 1. Sumario de las edades interpoladas de los límites de épocas y pisos del Devónico. Dataciones de edad radiométrica (según Agterberg et al., 2020).

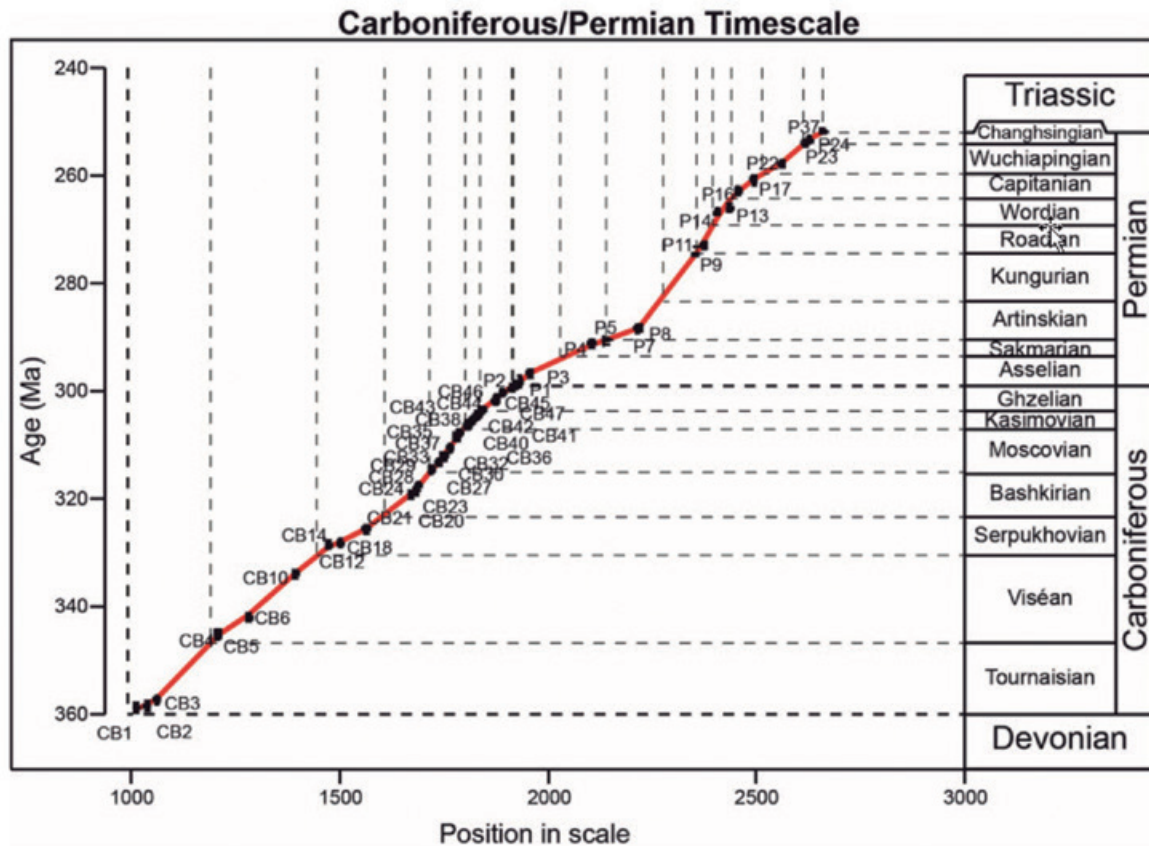


Figure 2. Best-fitting spline-curve for the Carboniferous-Permian in GTS2020.
Figura 2. Mejor ajuste de curvas por splines para el Carbonífero-Pérmico en GTS2020.

data for the Givetian and parts of its adjoining stages. It suggests that worldwide there exist gaps in the density distribution of age determinations along the stratigraphic scale. This may present a third source of uncertainty in time scale estimation that is independent of age determination errors and stratigraphic uncertainty. The original GST2012 data for the Devonian, which were also used by Vleeschouwer and Parnell (2014), will be used in the next two sections to investigate the possibility of spatial clustering of Devonian ash beds used for the age determinations.

Table 1 is a summary of interpolated ages of Devonian epoch and stage boundaries in:

- GTS2012, using cubic splining and cross-validation, with bootstrapped error bars (one-sided).
- GTS2020 data, using *R* cubic splining, clustering analysis and cross-validation (Figure 2).
- GTS2012, using Bchron and clustering analysis.

There is no significant difference in age estimates using *R* cubic splining+ or Bchron+, with stage durations also being comparable. The main difference in results obtained by these two different methods is that

the Bchron 95% error bar width shows rapid fluctuations in its width. It contains about ten local maxima in places of minimal density of occurrences of samples that were dated. Differences in error bar values are difficult to assess, but Bchron assigns relatively large uncertainty where there is a lack of age dates around or on one side of the interpolated age of a stage boundary. In the latter case Bchron appears to squeeze zones too much, in excess of their (thickness) duration uncertainty. The *R* cubic splining methods honour zonal stratigraphic uncertainty more, limiting how far a stage can expand in time. The mention of (thickness) in parenthesis just before the previous sentence is a reference to the fact that the Devonian position scale axis for the splines is derived from a subjective estimate of the duration of the Devonian zones and their link to the stage boundaries using relative thickness estimates. More information is provided by Becker et al. (in press) for GTS2020. The other Paleozoic periods, with the exception of the Cambrian that has no scaling of zones and stages, use different quantitative or semi-quantitative methods for stratigraphic compos-

Base of Stage	Dist (km)	Spline Age	2-Sigma	Duration	C-duration	Duration-2	Age-2	Final Age	2-Sigma
Cenomanian		~100.5	0.14				100.50	100.5	0.1
Albian		~113.1	0.30	12.60	12.45	12.84	113.34	113.2	0.3
Aptian	0	122.77	0.90	9.67	8.10	8.35	121.69	121.4	0.9
Barremian	120	127.23	0.78	4.46	5.00	5.16	126.85	126.5	0.8
Hauterivian	198	130.13	0.72	2.90	5.93	6.12	132.96	132.6	0.7
Valanginian	347	135.67	0.63	5.54	5.06	5.22	138.18	137.7	0.6
Berriasian	523	142.21	0.62	6.54	5.27	5.43	143.62	143.1	0.6
Tithonian	701	148.82	0.71	6.61	5.67	5.85	149.46	148.9	0.7
Kimmeridgian	845.2	154.18	0.84	5.36	5.20	5.36	154.83	154.8	0.8
Oxfordian	1013.69	160.44	1.03	6.26	5.80	5.98	160.81	160.8	1.0
Callovian	1082.58	163.00	1.11	2.56	3.00	3.09	163.90	163.9	1.1

Table 2. Late Jurassic and Early Cretaceous spline-curve age estimates adjusted for Milankovitch-based stage duration estimates (M-durations). Final Age estimates and 2-Sigma values are given in last two columns. See text for further explanations.

Tabla 2. Edades estimadas por ajuste de curva por splines para el Jurásico Superior – Cretácico inferior para estimaciones de duración de pisos basada en Milankovitch (M-duraciones). Estimaciones de edad final y valores 2-sigma se dan en las dos últimas columnas. Ver el texto principal para explicaciones.

iting to calculate a linear scale along the stratigraphic axis of events, zones and stages. Hence, such a linear stratigraphic scale can be compared to the scale with radiometric ages in a two-ways plot, using the splines, under discussion here.

A newly derived Devonian smoothing spline (Figure 4) using the earlier GTS2012 data results in estimated stage boundary ages that are close to those shown in Table 1. This is because it closely resembles the GTS2012 bootstrap spline. The latter was modified by connecting the dates for samples D7 and D9 with a straight-line segment. The new spline of Figure 4 is intersected by the 2-sigma error bars of all input dates except by those for dates D5 and D13/D14. A minor modification in the input data consisted of combining the dates for D13 and D14 into a single because they have the same position in stratigraphic scale according to the following method.

Suppose that y_i and y_{i+1} are two successive values with the same x -value. Their approximate 95% confidence interval can be written as $2 \times \sigma(y_i)$ and $2 \times \sigma(y_{i+1})$. From these two values, the weights of the two observations can be computed as $w_i = 1/\sigma^2(y_i)$ and $w_{i+1} = 1/\sigma^2(y_{i+1})$. The sum of these two weights can be written as $w(x) = w_i + w_{i+1}$ where x represents location of both y_i and y_{i+1} along the x -axis. The same procedure can be followed when more than two dates have the same value of x . If there are two dates only, their weighted average is

$$y_x = \frac{w_i y_i + w_{i+1} y_{i+1}}{w(x)}$$

Again, the same procedure can be followed if there are more than two dates with the same value of x . Application of this procedure to the GTS2020 age determinations for the Devonian (Figure 1) reduces the total number of dates from 31 to 19.

The preceding statistical procedure also can be used for combining two different estimates at a series

boundary. For example, the GTS2020 spline curves for the Devonian and the Carboniferous-Permian produced slightly different estimates for base Tournaisian (358.8 +/- 0.7 Ma and 359.9 +/- 0.4 Ma, respectively). The weighted average of these two estimates (359.3 +/- 0.3) is probably the best estimate of the age of the base of the Carboniferous. It is somewhat closer to 359.9 Ma with less uncertainty than 358.8 Ma. Likewise, the smoothing spline estimate for the GTS2020 base of the Devonian is 420.6 ± 1.2 Ma, whereas combined spline-curves for Silurian graptolites and conodonts yield 419.8 ± 1.5 Ma for this period boundary. The weighted average of these two estimates that is 420.3 ± 0.9 Ma can be taken as the best estimate for the Silurian-Devonian period boundary.

Statistical distribution of age determinations along the geologic time scale

How much weight should be given to the specific location of an age determination along the stratigraphic time scale? This is a philosophical question that suddenly has become important in GTS construction because of the conceptual modeling on which the Bchron algorithm is based.

Conceptually, we believe that differences of expected frequency of age determinations per unit of geologic time probably exist. For example, the 29 ⁴⁰Ar/³⁹Ar bentonite dates of Obradovich (1993) for the Late Cretaceous do not seem to be uniformly distributed. Within the 65 to 100 myr time interval, only 7 dates occur within the 65 to 82.5 myr time interval versus 22 within the 82.5 to 100 myr interval. If the bentonites that were dated would be randomly distributed over the entire 35 myr time interval, the probability of it occurring in the younger time interval is 0.5. The probability that only 7 (of the 29) would occur within this interval becomes 0.0029 and the probability of 7 or fewer than 7 is 0.0041. Both these probabilities

Stage Base	Spline-age	2-Sigma	Duration	C-Duration	Adjusted	Final Age
Tournaisian	359.3	0.3				359.3
Famennian	371.4	0.6	12.1	13.5	15.4	374.7
Frasnian	379.0	0.9	7.7	6.5	7.4	382.1
Givetian	385.9	1.5	6.9	4.4	5.0	387.1
Eifelian	394.2	1.6	8.2	6.2	7.1	394.2
Emsian	407.9	1.0	13.7			407.9
Pragian	414.4	1.1	6.5			414.4
Lochkovian	420.3	0.9	5.9			420.3
		T-E sum	34.9	30.6	34.9	

Table 3. Method illustrated for Late Jurassic and Early Cretaceous in Table 2 applied to post-Eifelian stages of the Devonian.

Tabla 3. Método ilustrado para el Jurásico Superior – Cretácico Inferior en la tabla 2 y aplicado a los pisos posteriores al Eifelense para el Devónico.

are less than 0.05 or 0.01. This suggests that there are probably fewer dates in the 65 to 82.5 Ma interval (and more in the 85.5 to 100 Ma interval) than expected for a random Poisson-type distribution. The probability of occurrence of a bentonite in the Late Cretaceous probably therefore depends on its age but how could we describe its time-dependent probability function?

In BChron, the estimated probability of a predicted age being correct is relatively large at the place of occurrence of a dated rock sample and even somewhat larger if nearby there are other dated rock samples, but why? The original GTS2012 Devonian time scale was based on only 19 irregularly distributed dates. Any discrete statistical model to test for systematic

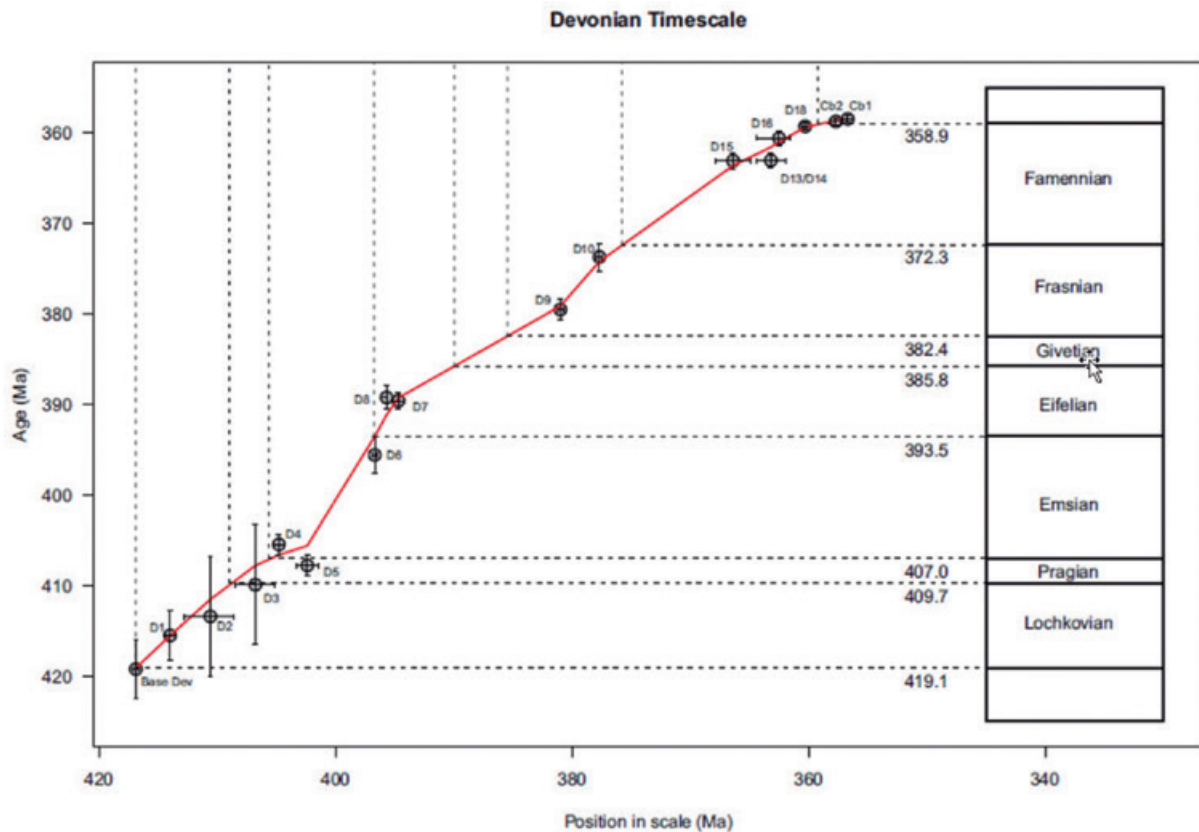


Figure 3. Devonian time scale based on smoothing spline fitted to GTS2012 age determinations and stratigraphic uncertainties.

Figura 3. Escala de tiempo para el Devónico basado en el ajuste por splines con suavizado para las determinaciones de edades GTS2012 e incertidumbres estratigráficas.

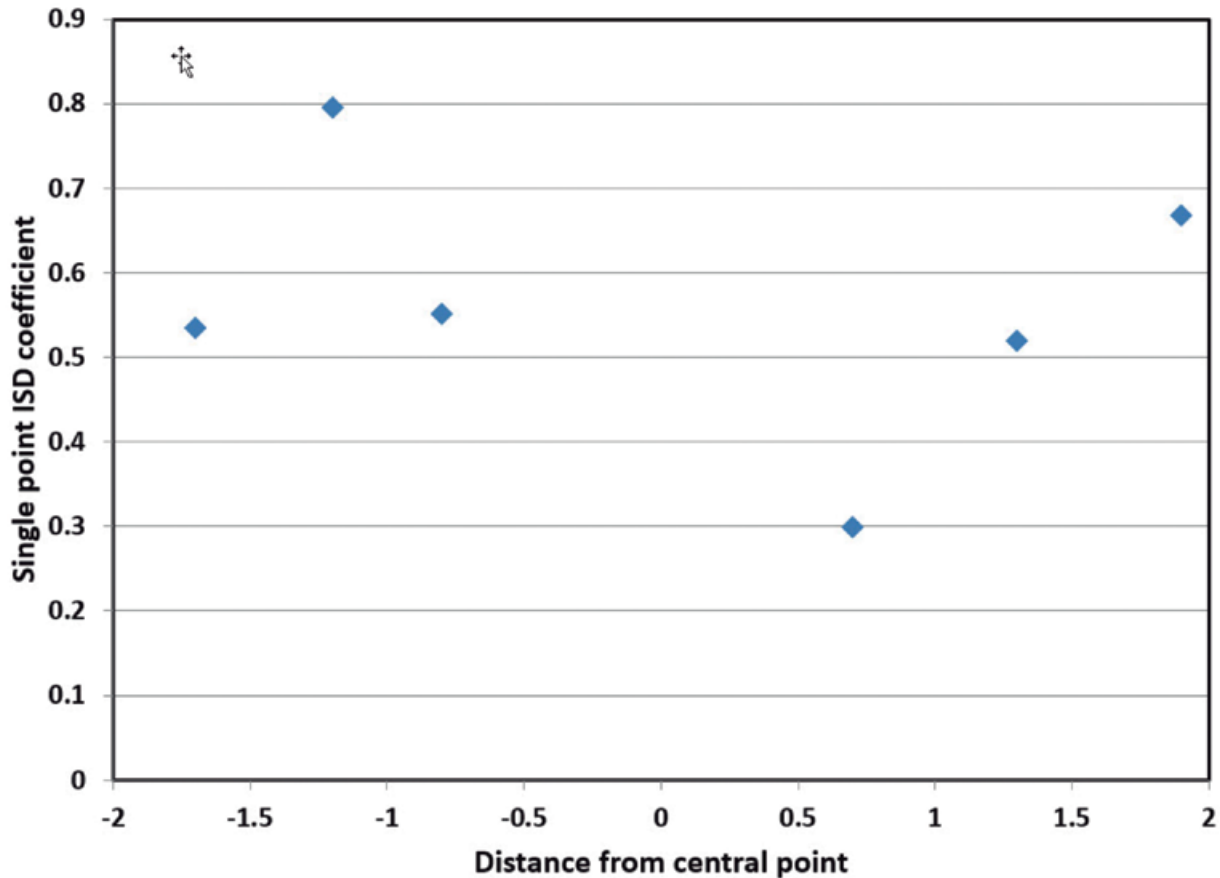


Figure 4. Example of coefficients derived for quadratic power-law model connecting age determination with $x = 17$ to its three neighbors along the relative stratigraphic scale on each side (older and younger). Average coefficient of these six values is shown at point with Dev1 in Figure 3.

Figura 4. Ejemplo de los coeficientes derivados para un modelo de ley potencial cuadrática conectando las determinación de edades con $x = 17$ a sus tres vecinos a lo largo de la escala estratigráfica y a ambos lados (más antiguo y más moderno). El coeficiente medio de estos seis valores se muestra en el punto con Dev1 en la Figura 3.

changes in a number of dates per unit of time would not indicate significant clustering in time because sample size is too small. We could, however, look at differences between dates along the Devonian time scale. The following (purely hypothetical) example illustrates why this may provide a more promising approach. Suppose that in a large study area the same ash layer is sampled twice at locations that are relatively far removed from one another. The age determinations for these two ash samples may be different but they would have exactly the same position along the relative geologic time scale. If a random distribution model is used for location of points, the probability that two age determinations would exactly coincide along the time scale is infinitesimally small. A definite result of this type could not be obtained from the original data when a Poisson-type model is used because the sample is too small. This is the reason that it will be good to look at first-order differences between loca-

tions of age determinations instead of at the locations themselves.

Simple power-law models are often used for the construction of contour maps for noisy geochemical data irregularly distributed across a study area. The most popular model along these lines is quadratic $\hat{y}_k = \frac{1}{n} \cdot \sum_{i=1}^n c_k \cdot y_{ik} \cdot d_{ik}^{-2}$ where the n values y_{ik} represent all observations located within a circular area with predefined radius around point k with estimated contour value at its center, and d_{ik} is the distance between the points of occurrence of y_k and y_{ik} . In our application this isotropic squared deviation (ISD) model can be used as follows. Every age determination y_k occurs at distance d_{ik} from other age determinations y_{ik} in its neighborhood. For example, the age determination y_k with value x_k along the geologic distance scale is distances d_{ik} removed from its closest neighbors with locations $x_{ik} = c_k \cdot (x_k - x_{ik})^{-2}$. Use is made of the fact that x_{ik} already represents an estimate of y_{ik} . For convenience,

a simplified linear scale was used instead of original position along the stratigraphic scale for the Devonian in GTS2012. There is a linear relation between the stratigraphic scale of Figure 4 and the horizontal scale in Figures 5 and 6 in which $x_k = 17$ represents sample D1 and $x_k = 136$ represents Cb1. The central point in Figure 5 with horizontal coordinate equal to 0 represents the point with $x_k = 17$. The six other points in Figure 5 represent the three closest neighbors at either side of x_k . In order to reduce edge effects, the series of 18 age determinations was enlarged at both the base and top of the Devonian using the end-point reflection technique often used in time series analysis. If there would be no clustering of x_k values, all values c_{ik} would be realizations of the same random variable and independent of choice of x_k value with its neighbor's x_{ik} .

Averages of c_k values within selected neighborhoods would also be the same if the points would occur randomly. The average of the six c_{ik} values shown in Figure 5 is $c_k = 0.657$. Figure 6 shows similar average

c_k values for all 18 x_k values. Standard deviations for all eighteen 6-point samples of relative ages were computed and multiplied by ± 1.96 to estimate 95% confidence limits for these average c_k values, which are also shown in Figure 5. Clearly there are significant differences between these values. It is noted that the version of the inverse square distance model used here is only applicable within relatively narrow neighborhoods. For x_k values within clusters of sampling points, wider neighborhoods could have been used; on the other hand, the choice of 3 neighbors on each side can be too wide for more isolated data points as illustrated by some points with unrealistic negative lower 95% confidence interval values shown in Figure 6. It can be concluded from the preceding exercise that the assumption of existing significant clustering in time of Devonian ages is reasonable. This tentative conclusion was confirmed to some extent in the following one-dimensional application of hot spot analysis.

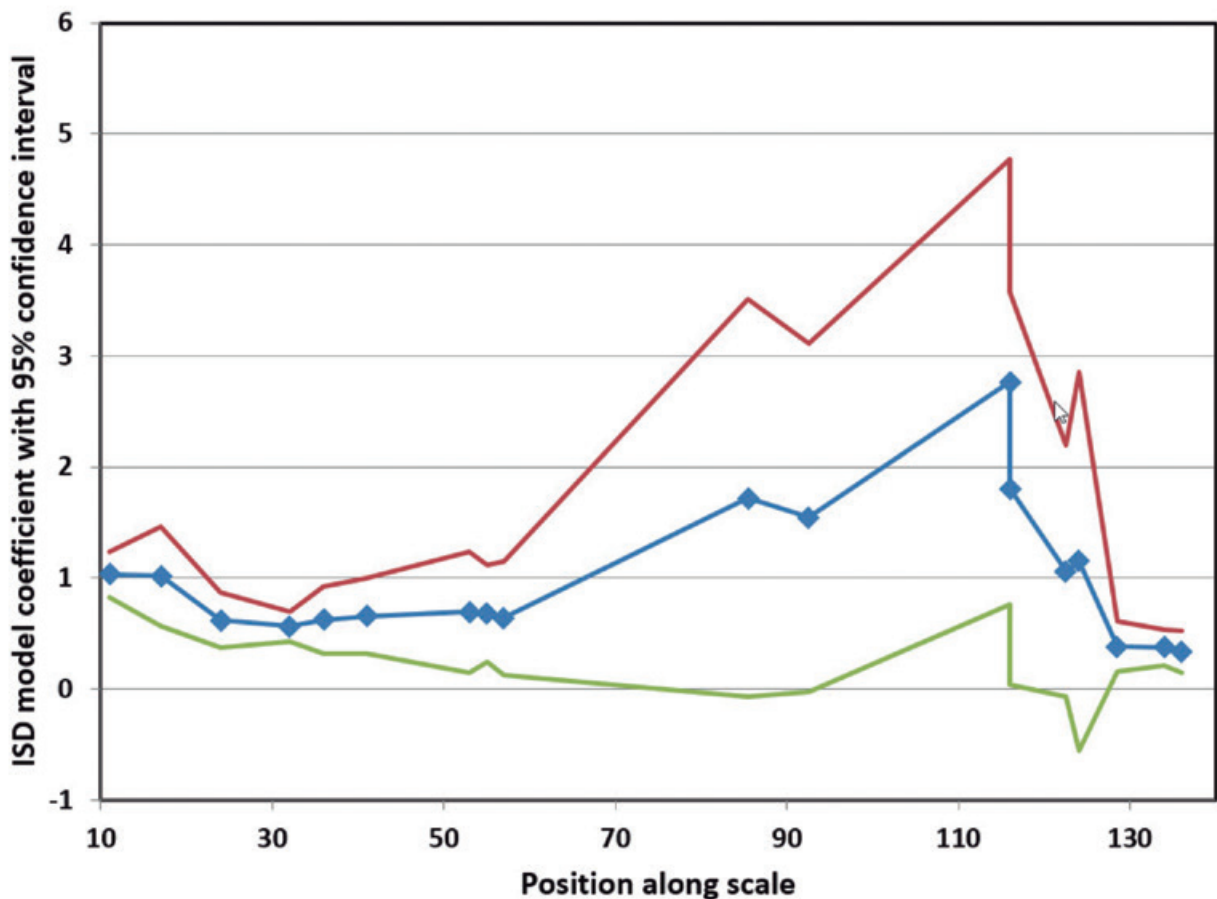


Figure 5. Estimated coefficients for separate applications of quadratic power-law model at every sampling point along the relative GST2012 Devonian time scale of Figure 3 with 95% confidence interval.

Figura 5. Coeficientes estimados para aplicaciones separadas del modelo de ley potencial cuadrática a cada punto a lo largo de la escala temporal relativa GST2012 para el Devónico de la Figura 3 con un intervalo de confianza del 95%.

Hot Spot Analysis

Hot spot analysis (see e.g. Getis and Ord, 1992) is widely applied by geographers to enhance two-dimensional patterns of random variables that exhibit spatial clustering. Typical examples are counts (x_{ij}) of occurrences (e.g. cases of a specific disease or accidents) for small areas (e.g. counties). Originally, the technique was based on Moran's I statistic for spatial correlation. It led to the Getis $G_i(d)$ statistic that satisfies:

$$G_i(d) = \frac{\sum_{j=1}^n w_{ij}(d)x_j}{\sum_{j=1}^n x_j}, j \text{ not equal to } i,$$

where $\{w_{ij}\}$ is an asymmetric one/zero spatial weight matrix with ones for all links defined as being within distance d of a given i , all other links being zero (cf. Getis and Ord, 1992, p. 190). Setting $W_i = \sum_{j=1}^n w_{ij}(d)$ it can be shown that the expected value of $G_i(d)$ and its variance satisfy:

$$E[G_i(d)] = \frac{W_i}{n-1}; \quad \sigma^2[G_i(d)] = \frac{W_i(n-1-W_i)Y_{i2}}{(n-1)^2(n-2)Y_{i1}^2}$$

where E denotes mathematical expectation, σ^2 is variance,

$$Y_{i1} = \frac{\sum_{j=1}^n x_j}{n-1}, \text{ and } Y_{i2} = \frac{\sum_{j=1}^n x_j^2}{n-1} - Y_{i1}^2.$$

Although this technique was developed for 2D applications, it can be used in 1D as well. We simply have to think of a rectangular area in 2D that is being compressed onto a 1D line segment. It implies that all distances between points become positive. Assuming that $G_i(d)$ is approximately normally distributed, the standard normal random variable becomes

$$Z_i = \{G_i(d) - E[G_i(d)]/\sigma[G_i(d)]\}$$

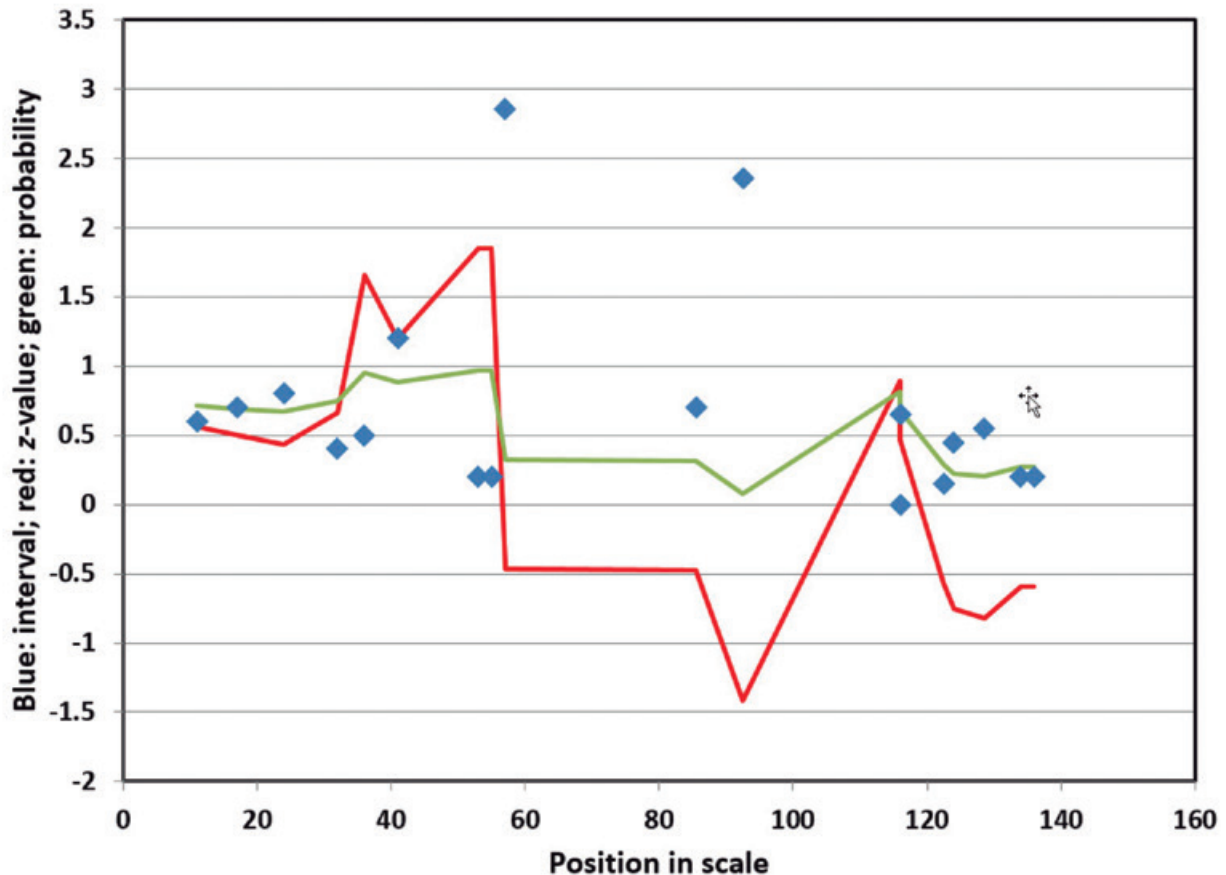


Figure 6. Results of 1D hot spot analysis. Local neighborhoods of the GTS2012 age determination locations were used to estimate z-values which are shown together with their standard normal probabilities

Figura 6. Resultados de análisis de punto caliente en 1D. Los vecinos locales de las localizaciones de determinación de edades GTS2012 se utilizaron para estimar z-values los cuales se muestran junto a sus probabilidades estándar normales.

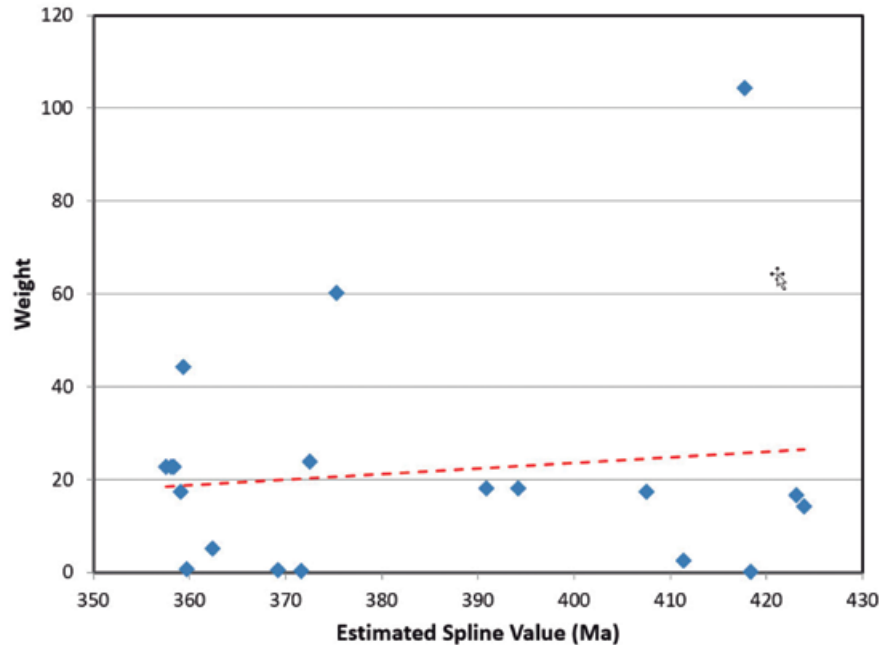


Figure 7. Weights of GTS2020 Devonian dates as a function of estimated spline value
Figura 7. Pesos de las dataciones de GTS2020 para el Devónico como una función del valor del spline estimado.

In the application to the relative age locations along the x -axis of Figure 4, weights for all distances less than 6.0 were set equal to 1, and all other weights were set equal to zero. Application of the preceding equations then results in the z -values graphically shown in Figure 7. Locally, these z -values almost reach the 95% confidence limit. As in the previous exercise that resulted in Figure 6, the possibility of clustering of ages along the horizontal scale is indicated. It is noted that anti-clustering locally is statistically significant at the 0.05 level of significance in the vicinity of the Givetian where density of age determinations is at its lowest. In the next section this fact will be used to modify the width of the 95% confidence belt on the best-fitting smoothing spline in Figure 2. It is also noted that the z -values and probabilities in Figure 7 show downward trends at the beginning and the end. These are end point effects that could have been reduced to some extent by application of the 1D end point reflection technique used to construct Figure 6.

New Approximate Devonian 95% Confidence Interval

The procedure of Paleozoic time scale construction followed in GTS2004 was based on the idea that a plot of the observed age determinations against the estimated spline ages is approximately according to a straight line with the simple equation $y = x$. This pro-

cedure is equivalent to the method originally used by McKerrow et al. (1985) and Cooper (1999). The 95% confidence belt for this line at any point (x_k, y_k) satisfies

$$y_k \pm t(n-2) \cdot s_e \sqrt{1 - R_k} \text{ where } R_k = \frac{1}{n} + \frac{(x_k - \sum x_k/n)^2}{\sum (x_k - \sum x_k/n)^2}$$

(cf. Agterberg, 1974, Equation 8.31).

The total number of observations $n = 19$ and Student's $t(17) = 2.11$. The Devonian weights used for the spline-fitting that resulted in Figure 1 are shown in Figure 8. There are two ways in which the standard deviation s_e can be calculated: weighted or unweighted. In the weighted method, which is to be preferred, every age determination is weighted according to the inverse of its variance. In the unweighted method all age determinations are given equal weights. In the current application the weighted method was used. Figure 9 shows the 95% half-confidence belt for the Devonian as a solid line. For the Devonian, the approach was taken one step further to account for the probable variations in density of sampling points investigated in the preceding section.

Suppose that m_k for point k is the number of other observations within a time interval of 10 myr. The maximum number of other observations within a time interval of 10 myr is $\max(m_k) = 7$. Density of observations for point k then can be set equal to $d_k = m_k / \max(m_k)$. The reciprocal of this measure of density

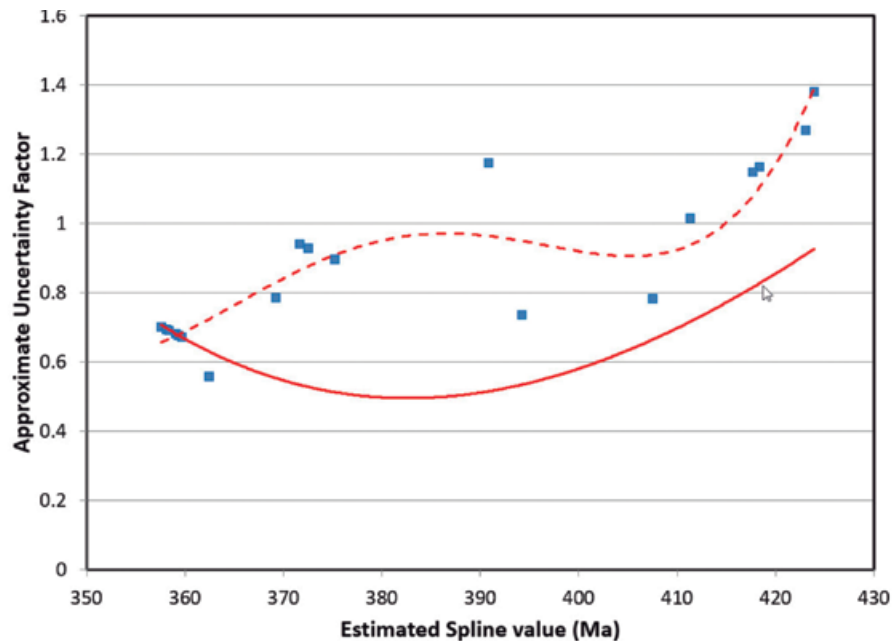


Figure 8. Approximate uncertainty factor used to widen 95% confidence belt incorporating changes of density of dates along the GTS2020 Devonian time scale.

Figura 8. Factor de incertidumbre aproximado utilizado para ampliar la banda con intervalo de confianza del 95% incorporando cambios de densidad de las dataciones a lo largo de la escala temporal GTS2020 para el Devónico.

provides a measure of sparseness of observations at any data point. Dividing the values of the 95% half-confidence interval results in the values shown in Figure 8 as solid squares. These values fall approximately on the broken line also shown in this figure. The broken line provides approximate 95% confidence intervals for the estimated ages of the GTS2020 Devonian stage boundaries shown in Table 1. In addition to the increases in uncertainty towards top and base of the Devonian, Figure 9 shows extra uncertainty at top and bottom of the Givetian where there is a relative lack of age determinations. The preceding procedure for the Devonian remains approximate and somewhat speculative because of lack of information.

Application to the Late Jurassic- Early Cretaceous

Spline-fitting as applied to Paleozoic periods in GTS2020 was also used to help obtain the GTS2020 Cretaceous time scale. The critical factor for the Early Cretaceous scale in GTS2020 is that a rather high resolution U-Pb radiometric, geomagnetic and cyclostratigraphic dataset is now available for the Tithonian through Barremian, not known during construction of GTS2012.

Figure 10 is a plot of radiometric age against mid km M-sequence values that span 1198.2 km in total. In order to incorporate stratigraphic uncertainty, $s(x)$ was estimated for each distance value (x) by multiplying its sigma value by the ratio of total time interval (= 47.8 myr) and the span of 1198.2 km in order to make use of the total variance equation: $s_t^2(y) = s^2(x) + s^2(y)$ (see Introduction). The resulting smoothing spline, which is also shown in Figure 10, is almost exactly a straight line representing constant seafloor spreading. The corresponding weights $W_t = 1/s_t^2(y)$ are given in Figure 11 and the deviations themselves are shown in Figure 12. These deviations are very small. The spline-curve in Figure 10 is approximately a straight line with the equation $y = 0.0372 \cdot x + 122.77$, a result that can also be obtained by using the method of ordinary least squares. Degree of fit for this line could not be improved significantly by including higher order terms in the polynomial equation fitted by the method of least squares.

Mid km M-sequence distances of stage boundaries are given in column 2 of Table 2 with the corresponding ages in column 3. These age estimates are also shown in Figure 10. It is noted that contrary to the Devonian period applications shown in Figures 2 and 4, relatively many uncertainty crosses do not intercept the best-fitting cubic spline curve. A probable

explanation of this fact is that the reported 2-sigma values of the age determinations are systematically too low. Nearly all uncertainties in the mid km M-sequence values are negligibly small. In GTS2004 Appendix 3 (Gradstein et al., eds., 2004) it was pointed out that, if all standard deviations of the dependent variable all too small by a factor c , the estimates of the two coefficients of the best-fitting straight line remain unbiased. It is only that their standard deviations, and their co-variance, are underestimated by the factor c . The doubly hyperbolic 95% confidence interval on the best-fitting straight line also would be too narrow (by the factor c). In order to avoid this problem and to obtain 2-sigma values of the stage base estimates we have followed the simple alternative method described previously (see section on estimation of approximate 95% Devonian confidence interval) by assigning equal weights to all data points plotted in Figure 10.

Kent and Gradstein (1985), in their Cretaceous and Jurassic geochronology study for the Decade of North America Geology publications arrived at constant and linear spreading of the M-sequence as a reasonable template to interpolate the Oxfordian through Barremian time scale. Despite use of few tie points for the age versus M-sequence km plot, the

Jurassic-Cretaceous boundary was interpolated by Kent and Gradstein (1985 and 1986) at 144 Ma, only slightly older than the current 143.1 ± 0.6 Ma.

Although the patterns of 2-dimensional distribution of points in Figures 10 and 11 are similar to patterns obtained for Paleozoic periods including the Devonian, the slightly different procedure (unweighted deviations from the spline-curve) was used for estimating the 95% confidence limits of the estimated Late Jurassic - Early Cretaceous stage boundary ages. As pointed out before, unweighted deviations from the spline were used instead of weighted deviations because the 2-sigma values for the dates are probably underestimated. Table 2 contains estimated spline ages for Aptian to Callovian stage bases for which mid km M-sequence values were available along with their estimated 2-sigma values.

In the next two columns of Table 2 durations according to the spline-curve are compared with Milankovitch-cycle duration estimates (C-Durations in Table 2) Although the spline ages are probably unbiased estimates of the true ages, the C-durations are probably better stage duration estimates. Much of the tuning of Aptian-Albian time has been based on the Piobboco core (Tiraboschi et al., 2009), drilled into pelagic and hemipelagic strata in the Umbria-Marche

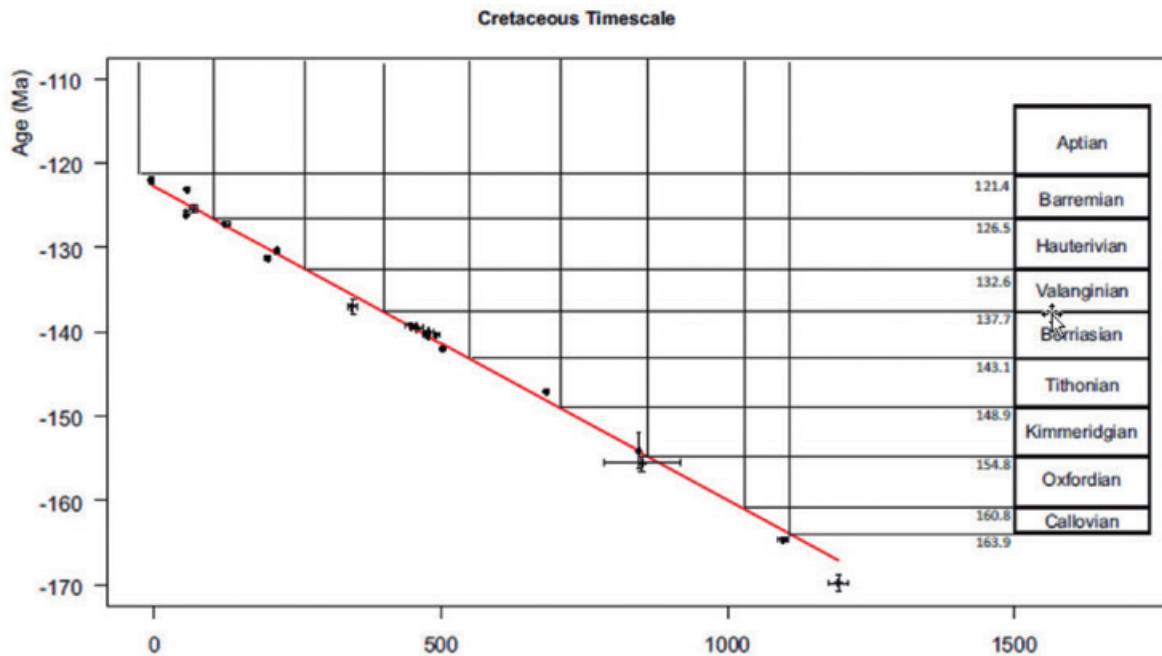


Figure 9. Best-fitting spline-curve for the Early Cretaceous in GTS2020.

Figura 9. Mejor ajuste de curva por splines para el Jurásico Superior – Cretácico Inferior en GTS2020.

Apennines, central Italy. Although the Albian duration, using cycles of 12.45 ± 0.5 is well established, the same is not the case for the Aptian. In GTS2012 a duration of 13.3 myr is now being contested and a shorter duration of 8.1 ± 0.5 is considered more likely and adhered to in this study. There is evidently a problem with the cyclostratigraphical interpretation of the lower part of the Piobboco core (Gale et al., in press).

Sums of durations from the Callovian to Albian (Table 2) are 63.40 myr (spline durations) and 61.48 (C-durations), respectively. The difference between these two sums of durations is 1.92 myr. Assuming that the Callovian and Albian age estimates are unbiased, the C-durations can be corrected so that their sum also becomes 63.40 myr. The resulting C-durations are listed in the Duration-2 column of Table 2. The resulting stage boundary ages are shown in the Age-2 column. However, when the summation is carried out from the Albian to the Oxfordian (instead of from the Albian to the Callovian) the spline age interval becomes 48.32 myr and the difference between sums of duration is reduced to 0.84 myr. Assuming that this estimate is unbiased, the M-durations can be adjusted so that their sum becomes 48.32 myr as well. The corrected M-durations then can be used to

estimate stage base age estimates between the Albian and the Oxfordian. These adjusted estimates together with the previously obtained estimates for the Kimmeridgian, Oxfordian and Callovian are shown as final age estimates in Table 2 along with the original spline-based 2-sigma values.

Milankovitch cycles for the Early Cretaceous are better established than those for the Paleozoic. Relatively reliable Milankovitch durations for four Devonian stages are listed in Table 3. Total duration estimates based on the spline-curve and sum of Milankovitch durations are 34.9 myr and 30.6 myr, respectively. If 34.9 myr would be accepted as the better estimate and used to correct the Milankovitch durations using the same method as that used for the Early Cretaceous, the final Devonian stage estimates would become as those shown in the last column of Table 3. These estimates differ from those previously given in Table 1.

Concluding remarks

Estimation of the ages of period and stage boundaries of the Geologic Time Scale (GTS) has a long history (Gradstein et al, eds., in press). This paper was con-

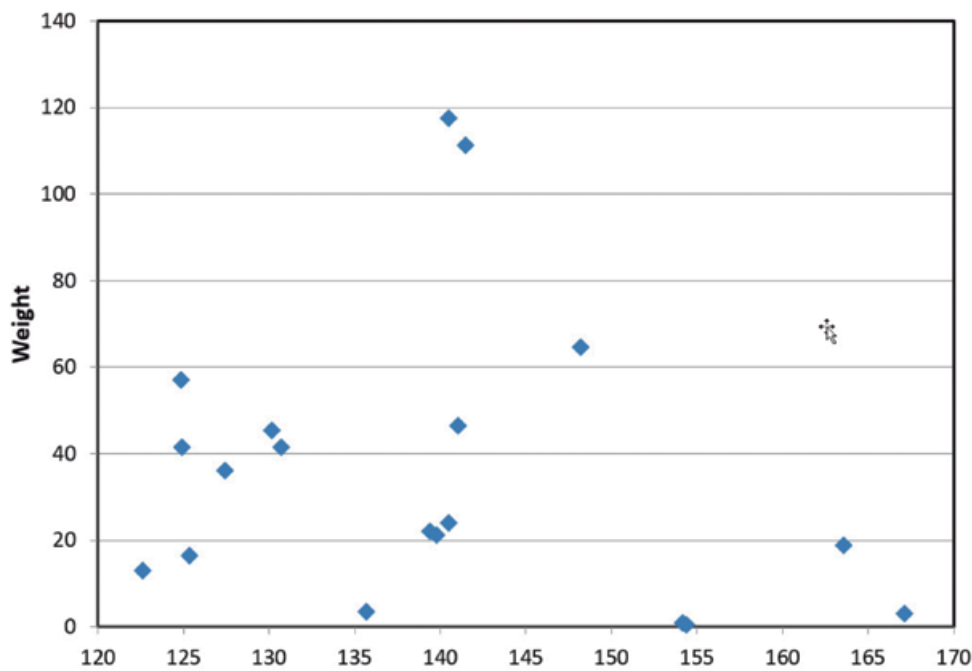


Figure 10. Weights of Early Cretaceous dates as a function of estimated spline values..

Figura 10. Pesos de las dataciones Jurásico Superior – Cretácico Inferior como una función de los valores estimados por splines.

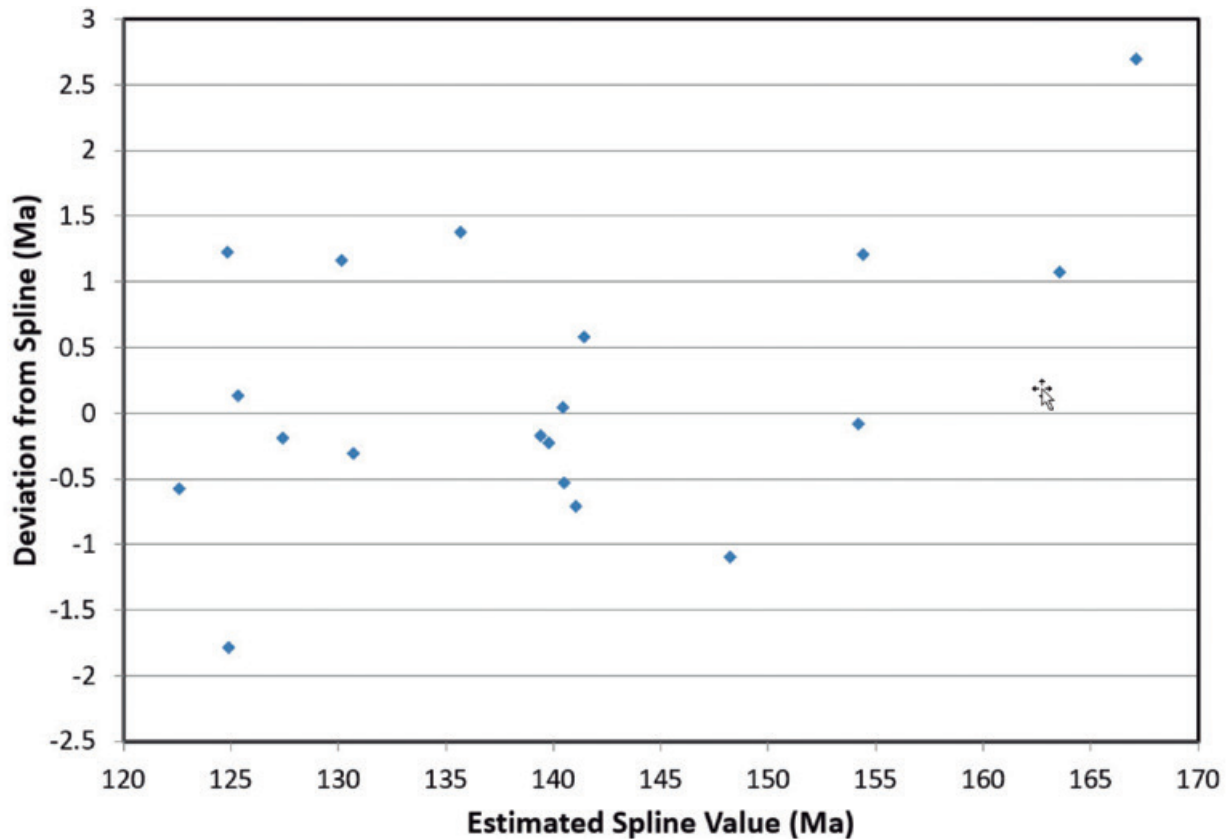


Figure 11. Deviations of input ages from spline-curve of Figure 9.

Figura 11. Desviaciones de las edades de entrada de la curva ajustada por splines de la Figura 9.

cerned with aspects of estimating the Devonian and Early Cretaceous time scales as used for GTS2020. The purpose of time scales remains to calculate the ages of stage boundaries (in Ma) and other events along the worldwide stratigraphic scale, which is relative, from reliable radiogenic isotope age determinations. Quantity and quality of the input information continues to increase steadily. If there remain significant uncertainty in the time scale age estimates these should be accompanied by error bars which are based on both the 2-sigma age dating errors and any stratigraphic uncertainties. Most GTS2004 and GTS2012 results involved spline-curve fitting but in GTS2012 Milankovitch-type orbital climate cyclicity was used to tune the Neogene geologic time scale while seafloor spreading was combined with sedimentary cycle scaling to construct the Paleogene time scale. Cycle scaling also contributed to the construction of the GTS2020 Cretaceous and Jurassic time scales.

Geomathematical procedures continue to be refined for GTS2020. In this study smoothing splines were used to construct Devonian and Early Cretaceous time scales. This methodology and its results were described and several estimates were refined by incorporating Milankovitch cycle durations. In addition to the 2-sigma dating errors and uncertainties in positions of the dated samples along the stratigraphic scale, geologic time clustering of dates was investigated as a third source of uncertainty for the Devonian which has a relative lack of input dates from the Late Eifelian to the Early Frasnian. Statistical significance of long-term fluctuations of this type was investigated using a 1-dimensional version of Getis-Ord hot spot analysis. It is likely that this additional source of uncertainty will become more important in future when more dates will become available. Likewise, Milankovitch-type orbital climate cyclicity probably will continue to improve the Mesozoic and Paleozoic time scales.

Acknowledgements

The authors are grateful to Dr. Alastair Ruffell and an anonymous reviewer for helpful comments that have improved the text of the paper.

References

- Agterberg, F.P. 1974. *Geomathematics*. Elsevier, Amsterdam, 596 pp.
- Agterberg, F.P. 2002. Construction of numerical geological time scales. *Terra Nostra*, 04/2002, 227-232.
- Agterberg, F.P. 2004. *Geomathematics*. In: Gradstein, F.M., Ogg, J.G. and Smith, A.G. (eds.), *A Geologic Time Scale 2004*. Cambridge University Press, Cambridge, pp. 106-125.
- Agterberg, F.P., Hammer, O. and Gradstein, F.M. 2012. In: Gradstein, F.M., Ogg, J.G., Schmitz, M.D. and Ogg, G.M. (eds.). *The Geologic Time Scale 2012*. Elsevier, Amsterdam, pp. 269-273.
- Becker, R.T. et al. in press. The Devonian. In: Gradstein, F.M. et al. (eds.), *A Geologic Time Scale 2020*.
- Chambers, J.M. and Hastie, T.J. 1992. *Statistical Models in S*. Wadsworth, S. and Brooks/Cole, London, 608 pp.
- Cooper, R.A. 1999. The Ordovician time scale - calibration of graptolite and conodont zones. *Acta Universitatis Carolinae Geologica*, 43(1/2), 1-4.
- De Vleeschouwer, D. and Parnell, A.C. 2014. Reducing time-scale uncertainty for the Devonian by integrating astrochronology and Bayesian statistics. *Geology*, 42(6): 491-494.
- Gale, A.S., Mutterlose, J. and Batenburg, S. in press. The Cretaceous. In: Gradstein, F.M. et al. (eds). *A Geologic Time Scale 2020*.
- Getis, A. and Ord, J.K. 1992. The analysis of spatial association by use of distance statistics. *Geographical Analysis*, 24(3): 189-206.
- Gradstein, F.M., Ogg, J.G. and Smith, A.G. (eds.) 2004. *A Geologic Time Scale 2004*. Cambridge University Press, Cambridge, 589 pp.
- Gradstein, F.M., Ogg, J.G., Schmitz, M.D. and Ogg, G.M., eds. 2012. *The Geologic Time Scale 2012*. Elsevier, Amsterdam, 1144 pp.
- Gradstein, F.M., Ogg, J.G., Schmitz, M.D. and Ogg, G.M., eds. 2020. *The Geologic Time Scale 2020*. Elsevier, Amsterdam.
- Hastie, T.J. and Tibshirani, R.J. 1990. *Generalized Adaptive Models*. Chapman and Hall, London, 328 pp.
- Harland, W.B., Cox, A.V., Llewellyn, P.G., Pickton, C.A.G. Smith, A.G. and Walters, R. 1982. *A geologic time scale*. Cambridge University Press, Cambridge, 131 pp.
- Harland, W.B., Armstrong, R.L., Cox, A.V., Craig, L.A., Smith, A.G. and Smith, D.G. 1990. *A geologic time scale 1989*. Cambridge University Press, Cambridge, 263 pp.
- Kent, D.V. and Gradstein, F.M. 1985. A Cretaceous and Jurassic geochronology. *Geol. Soc. America* 96, 1419-1427.
- Kent, D.V., and Gradstein, F.M. 1986. A Jurassic to Recent geochronology. In: Vogt, P.R. and Tucholke, B.E. (eds.), *The Geology of North America. Vol. M, The Western North Atlantic Region*. Boulder: Geological Society of America, 45-50.
- McKerrow, W.S., Lambert, R.S.J. and Cocks, L.R.M. 1985. The Ordovician, Silurian and Devonian Periods. In Snelling, N.J. (ed.), *The chronology of the geological record. Geological Society of London, Memoir* 10, 73-80.
- Obadovich, J.D. 1993. A Cretaceous time scale. In Caldwell, W.G.E. and Kaufman, E.G. (eds.), *Evolution of the Western Interior Basin*. Geological Association of Canada Special Paper, 379-396.
- Schwarzacher, W. 1993. *Cyclostratigraphy and the Milankovitch theory*. Elsevier, Amsterdam, 225 pp.
- Tiraboschi, D., Erba, E. and Jenkyns, H.C., 2009. Origin of rhythmic-Albian black shales (Piobboco core, central Italy): Calcareous nannofossil quantitative and statistical analysis and paleoceanographic reconstructions. *Paleoceanography and Paleoclimatology* 24, 23 June 2009.
- Wahba, G. 1985. A comparison of GCV and GNL for choosing the smoothing parameters in the generalized spline smoothing problem. *Annals of Statistics* 4, 1378-1402.
- Wang, Y. 2011. *Smoothing splines. Methods and applications, Monographs on Statistics and Applied Probability*, 121. CRC Press, Boca Baton, Florida, 370 pp.

Recibido: julio 2019

Revisado: noviembre 2019

Aceptado: enero 2020

Publicado: marzo 2021